NASA/TM– 20240002116

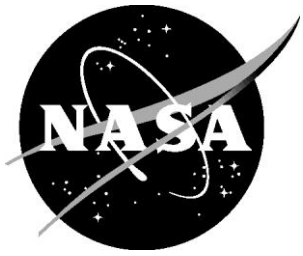

Fundamental Proprotor Design Considerations

Nathaniel J. Blaesser
Langley Research Center, Hampton, Virginia

December 2024

NASA STI Program Report Series

Since its founding, NASA has been dedicated to the advancement of aeronautics and space science. The NASA scientific and technical information (STI) program plays a key part in helping NASA maintain this important role.

The NASA STI program operates under the auspices of the Agency Chief Information Officer. It collects, organizes, provides for archiving, and disseminates NASA's STI. The NASA STI program provides access to the NTRS Registered and its public interface, the NASA Technical Reports Server, thus providing one of the largest collections of aeronautical and space science STI in the world. Results are published in both non-NASA channels and by NASA in the NASA STI Report Series, which includes the following report types:

- TECHNICAL PUBLICATION. Reports of completed research or a major significant phase of research that present the results of NASA Programs and include extensive data or theoretical analysis. Includes compilations of significant scientific and technical data and information deemed to be of continuing reference value. NASA counterpart of peer-reviewed formal professional papers but has less stringent limitations on manuscript length and extent of graphic presentations.

- TECHNICAL MEMORANDUM. Scientific and technical findings that are preliminary or of specialized interest, e.g., quick release reports, working papers, and bibliographies that contain minimal annotation. Does not contain extensive analysis.

- CONTRACTOR REPORT. Scientific and technical findings by NASA-sponsored contractors and grantees.

- CONFERENCE PUBLICATION. Collected papers from scientific and technical conferences, symposia, seminars, or other meetings sponsored or co-sponsored by NASA.

- SPECIAL PUBLICATION. Scientific, technical, or historical information from NASA programs, projects, and missions, often concerned with subjects having substantial public interest.

- TECHNICAL TRANSLATION. English-language translations of foreign scientific and technical material pertinent to NASA's mission.

Specialized services also include organizing and publishing research results, distributing specialized research announcements and feeds, providing information desk and personal search support, and enabling data exchange services.

For more information about the NASA STI program, see the following:

- Access the NASA STI program home page at http://www.sti.nasa.gov

NASA/TM– 20240002116

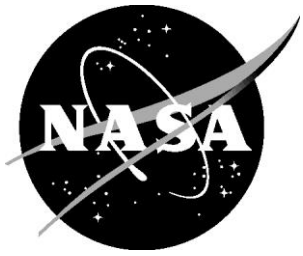

Fundamental Proprotor Design Considerations

Nathaniel J. Blaesser
Langley Research Center, Hampton, Virginia

National Aeronautics and
Space Administration

Langley Research Center
Hampton, Virginia 23681-2199

December 2024

Acknowledgements

The author thanks Siena Whiteside, Brandon Litherland, and Jason Welstead of NASA's Langley Research Center for their support and feedback during this effort. The author also thanks Wayne Johnson and Chris Silva of NASA's Ames Research Center for their guidance and expertise on rotorcraft and past rotor and proprotor design considerations. This research was funded by the Revolutionary Vertical Lift Technology project under the Advanced Air Vehicles Program.

Available from:

NASA STI Program / Mail Stop 050
NASA Langley Research Center
Hampton, VA 23681-2199

Abstract

The purpose of this technical memorandum is to document some of the fundamental considerations in the aerodynamic design of a proprotor blade, which include distributions of twist, chord, and thickness. A proprotor is expected to operate efficiently in different speed regimes, such as hover and forward flight, which presents challenges that are unique from designing either rotors or propellers. Operating in hover and at high advance ratios in cruise present conflicting design requirements on the blade's geometry that must be reconciled with the vehicle's mission. Though a proprotor must also fly in edgewise and other non-axial flight phases, these portions of the mission do not typically drive the proprotor's aerodynamic design. This memorandum describes an approach to integrate a blade's twist and chord distributions to provide an aerodynamic performance estimate that could be coupled with other design considerations, such as acoustics or structures. The intended audience for this memorandum is engineers beginning to work in this discipline who are looking for a primer on the behavior of proprotor performance and design considerations. The memorandum is not intended as a step-by-step guide to designing proprotors, nor does it provide insight into more advanced proprotor design/analysis tools.

Nomenclature

A	=	Area
A_b	=	Blade area
B	=	Number of blades
c	=	Chord
$c_{\{0,1,2\}}$	=	Chord distribution constants
C_{F_N}	=	Coefficient of normal force
C_{F_T}	=	Coefficient of tangential force
C_{L_α}	=	Airfoil lift curve slope
C_T	=	Thrust coefficient
L/D	=	Lift-to-drag ratio
N	=	Number of proprotors on vehicle
p_∞	=	Freestream pressure
Δp	=	Pressure rise across actuator disk
P_s	=	Shaft power
Q	=	Torque
r	=	Radial station
r_0	=	Radial station at the root
r_m	=	Radial station of maximum chord
R	=	Blade radius
V	=	Velocity
V_2	=	V downstream of actuator disk
V_∞	=	Freesteam velocity
$V_{\perp LE}$	=	V perpendicular to leading edge
α	=	Airfoil angle of attack
β	=	Geometric blade twist
η_p	=	Proprotor efficiency
θ	=	Blade pitch angle
θ_C	=	Blade collective setting
κ	=	Fraction of total thrust on a proprotor
λ_b	=	Blade taper ratio
λ	=	Langrange multiplier
μ	=	Advance ratio
ρ	=	Air density
σ	=	Rotor solidity
ϕ	=	Inflow angle
$\phi_{3/4}$	=	ϕ at $r/R = 0.75$
$\Delta\phi$	=	Change in ϕ from blade root to tip
ω	=	Angular velocity
$\mathcal{T}$	=	Thrust
$\mathcal{L}$	=	Lagrangian function

1. Introduction

Within this technical memorandum, proprotors are defined as a set of blades that rotate about an axis that can convert its orientation relative to the vehicle depending on the phase of flight. For example, a proprotor may have its axis parallel to the gravity vector during takeoff and landing, but the axis converts to an orientation perpendicular to gravity during cruising flight. This definition is contrasted with propellers and rotors that have a fixed axis relative to the vehicle. On helicopters, the rotor's axis is always aligned (or nearly so) with the gravity vector; for airplanes, the propeller axis is always perpendicular (or nearly so) to the gravity vector. Proprotors are found on numerous aircraft concepts, such as the tiltwing [1] or tiltrotor [2] vehicles shown in Fig. 1. This memorandum is not specific to a type of vehicle, nor does it describe broader vehicle design considerations.

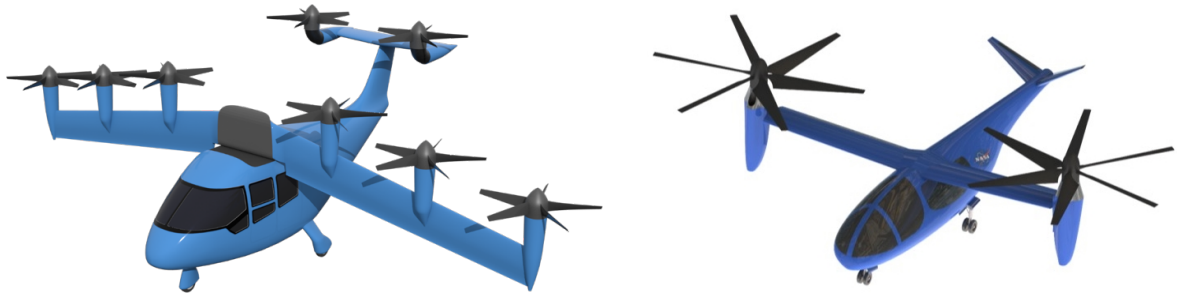

(a) Tiltwing [1]

(b) Tiltrotor [2]

Figure 1: Examples of tiltwing and tiltrotor reference aircraft that utilize proprotors.

This memorandum considers only the aerodynamic aspects of proprotor design. Other facets, such as acoustics, structures, or even proprotor-wing interactional effects, are not discussed herein. The intent of this memorandum is to explain some of the basic vocabulary and flow phenomenon related to the aerodynamics of proprotors. In understanding the fundamentals, readers will understand what limits proprotor performance and why proprotor design remains a challenge.

There have been numerous papers that describe proprotor analysis [3–7], especially for a single discipline such as aeroacoustics, but there are relatively few papers that describe the design of the proprotor. Recently, Gur wrote a book on propeller design that includes many important considerations within that discipline, though he does not address proprotors specifically [8]. Similarly, many papers in the literature feature design studies wherein specific design cases are analyzed, but they do not help the reader understand how the study can be extrapolated to another study. These statements are not meant to be critical; each paper is written for a specific intent. But none are focused on the education of blade physics required to make design decisions. Perhaps the best design example is by McVeigh et al., where the team discussed the process and trades that led to the XV-15 blade design [9]. More recently, Bain, Mikić, and Stoll described the design of the Joby proprotors, though the paper intentionally omits key details to protect Joby's intellectual property [10].

Within this memorandum, a proprotor design consists of the number of blades, twist distribution, and chord distribution. There are other parameters that one can control such as the material used or the method of construction. If the blades are made of carbon fiber, one can also control the direction of the layup to affect the structural properties. Similarly, the blade shape is only one piece of a larger system. A blade must be integrated into a hub with hinges, dampers, controllers, and other subsystems to operate in its desired state. This report neglects all other integrated subsystems or design considerations beyond the blade count and shape.

2. Aerodynamic Considerations

A. Low-Order Approximations

The overall goal of a proprotor design is to minimize the installed power and energy consumption for the vehicle while meeting the thrust requirements in all phases of flight. The dominant phases of flight with respect to these two metrics are hover and forward flight, with hover requiring the largest power consumption and forward flight typically consuming the largest portion of energy. Most vertical takeoff and landing (VTOL) vehicles have a defined "conversion corridor" that defines the proprotor axis angle and forward velocity as the VTOL transitions from hover to forward flight.[1] Other operating phases—edgewise flight or conversion between hover and forward flight—do not constrain the proprotor's aerodynamic performance, though edgewise flight does present structural loads that may constrain the proprotor design or limit its performance. Twist and taper do not impact the top of the conversion corridor enough to warrant its consideration in the initial blade design. The thrust requirements at hover are to balance the vehicle's weight and download. At cruise, the thrust must balance the drag at the desired airspeed. The thrust levels, $\mathcal{T}$, at each phase are loosely related through the vehicle's lift-to-drag ratio, L/D, via Eq. (1) because at hover lift equals weight, and at cruise, thrust equals drag.

$$\mathcal{T}_{cruise} \approx \frac{\mathcal{T}_{hover}}{L/D} \tag{1}$$

The first phase in assessing the proprotor design is determining the solidity and proprotor diameter. Helicopters have historical ranges for disk loading, defined as the thrust per unit of area swept by the blades, that can be used as an initial estimate for sizing disk area for the hover condition. The simplest proprotor loading model, momentum theory, treats the proprotor as an actuator disk with a constant pressure jump over its swept area. Equation (2) defines the thrust in terms of the pressure jump, Δp, and swept area, A. Per Eq. (2), the disk loading is equivalent to Δp for an actuator disk.

$$\mathcal{T} = A\Delta p \tag{2}$$

In forward flight the proprotor acts like a propeller, and we can use one-dimensional flow continuity to define a proprotor's maximum Froude efficiency via Eq. (3).[2] Within Eq. (3), η_p is the proprotor efficiency, V_∞ is the freestream velocity, and ρ is the air density. If the vehicle's thrust and forward speed are known, we can trade proprotor efficiency for proprotor diameter.

$$\eta_p = \frac{2V_\infty}{V_\infty + \sqrt{\frac{2\mathcal{T}}{A\rho} + V_\infty^2}} \tag{3}$$

A flaw in applying Eq. (3) is that modeling the proprotor as a constant pressure jump neglects the power lost to viscous effects on the blade. Effectively, Eq. (3) assumes the proprotor has an infinite number of blades where each blade consists of a lifting line. A lifting line has no chord and consequently has no viscous drag or its corresponding power loss. For proprotors (and propellers and rotors) solidity, σ, is used to express how much of the swept area is physically occupied by a blade. Solidity is defined as the ratio of blade area to disk area, though the solidity is often

[1] Within Ref. [11], Fig. A.7 shows the conversion corridor for the XV-15 tiltrotor research aircraft.

[2] Appendix A contains a more complete derivation of Eq. (3).

thrust-weighted to account for non-rectangular blade profiles.[3] Equation (4) shows a basic, non-thrust-weighted, rotor solidity for a proprotor where B is the number of blades, A_b is the area of a single blade, and R is the blade radius. Equation (5) shows the equation for the area of a single blade, which is dependent on the chord distribution, $c(r)$, from root, r_0, to tip, R. For proprotors with low solidity, Eq. (3) may be a valid approximation; but as solidity increases—and proprotors have high solidity due to hover requirements—Eq. (3) may not be appropriate. Because of the effects of solidity, the Froude efficiency will always be optimistic, and the actual efficiency will be lower than predicted by Eq. (3). Thus, the resulting disk area is a minimum for the proprotor for a given target efficiency.

$$\sigma = \frac{BA_b}{\pi R^2} \tag{4}$$

$$A_b = \int_{r_0}^{R} c(r)dr \tag{5}$$

During hover, the inflow velocity is low enough that the Froude efficiency approximation fails. Instead, the figure of merit (FoM) metric is used and is defined as the ideal power required to hover divided by the actual power required to hover. The ideal power comes from momentum theory and therefore does not include viscous losses. For this reason, the FoM is always less than one. A good FoM is usually similar to, but lower than, a good η_p, with a typical value being around 0.7.

B. Mission Considerations in Design

Hover thrust requirements will be greater than forward flight thrust requirements, and it is this disparity that creates the central challenge to designing an effective proprotor. The means of adjusting thrust is to change the rotor speed—the rotor's revolutions per minute (RPM)—or the proprotor collective (or pitch setting if using propeller terminology). Ultimately, rotor speed and collective setting control the angle of attack that a blade's airfoil will experience. The proprotor will be most efficient when the blade sections' airfoils are operating closest to their maximum L/D. As the collective is changed and the operating point is moved away from the airfoils' maximum L/D, the proprotor's efficiency will decrease. The balance of designing the proprotor for hover or cruise therefore depends on the mission of the vehicle.

The blade loading coefficient is defined as the thrust coefficient, C_T, normalized by the rotor solidity, σ. Thrust coefficient, defined by Eq. (6), is the proprotor's thrust, $\mathcal{T}$, normalized by density, ρ, disk area, A, and the square of the proprotor's tip speed, ωR. The tip speed is the product of the rotor speed, ω, and the blade's radius, R.

$$C_T = \frac{\mathcal{T}}{\rho A(\omega R)^2} \tag{6}$$

Leishman notes that C_T/σ is limited to an upper value of approximately 0.12 [12]. This limit comes from the airfoil section's maximum lift coefficient. The metric of C_T/σ, when calculated out and expressed in its simplest form, effectively becomes the integrated lift coefficient across the blade. Thus, the upper limit comes from the stall behavior of the proprotor's airfoils. Using this limit sets the minimum solidity that the proprotor can have for a given C_T. Setting a minimum solidity is a necessary first step because aerodynamic solvers will always push to have smaller chords in an attempt to reduce viscous power losses, especially if a proper stall model is not implemented.

[3] Leishman describes in greater detail the reasons for, and means of, calculating weighted solidity through blade element momentum theory in Ref. [12].

The number of proprotors is also a design parameter, which can be varied such that the three metrics cited above—disk loading, proprotor efficiency, and blade loading—fall within historical norms. Proprotors of different sizes or blade counts can be used. Appendix B shows, at least for an ideal proprotor in axial flight, that the system's Froude efficiency is maximized when the disk loading across the proprotors is held constant regardless of disparities in rotor size.

With the overall disk area and loading identified, we can move on to individual blade performance, beginning with twist distribution.

C. Aerodynamics of Edgewise Flight

Edgewise flight does not influence the proprotor design, but it is still worthwhile to discuss its aerodynamics. Edgewise flight aerodynamics are relevant because many VTOL platforms adopt helicopter terminology and limits on flight speeds in edgewise flight provide the motivation for using tiltwing or tiltrotor platforms. The following section describes some of the challenges with edgewise flight to orient the reader and to introduce the concept of advance ratio for rotors and propellers.

Equation (7) defines the advance ratio, μ, where V_∞ is the forward velocity and ω is the proprotor's rotational velocity in radians per second.[4] Because Eq. (7) is using the "helicopter" definition of advance ratio, the freestream velocity is perpendicular to the proprotor's rotational axis, i.e., in edgewise flight.

$$\mu = \frac{V_\infty}{\omega R} \tag{7}$$

For helicopters in edgewise flight, maximum advance ratio is below one due to the flow direction the retreating blade experiences. Figure 2 shows a snapshot in time of a simplified proprotor in flight at a moderate advance ratio, with the observer above and looking down at the proprotor. The freestream velocity is coming from the top of the page and the proprotor's rotation direction is counterclockwise. Figure 2a shows the separate freestream and rotational velocity components. Figure 2b shows the resultant velocities across the leading edge, with a small region of reverse flow on the left side, near the hub. As the advance ratio increases—implying a greater freestream velocity while the rotational velocity is held constant—the region of reverse flow will grow, exacerbating the difference in dynamic pressure on the advancing and retreating blade.

Figure 3 shows contours of velocity perpendicular to the leading edge of the blade,[5] $V_{\perp LE}$, normalized by the tip velocity, ωR, for three different advance ratios. The $V_{\perp LE}$ term has the appearance of an advance ratio, though the similarity is superficial. What $V_{\perp LE}$ actually represents is the velocity that determines the section's thrust and drag, normalized by tip velocity. The normalization scheme helps show the radial variance in velocity from root to tip.

Within Fig. 3, the incoming velocity is coming down from the top of the image, and the rotor is rotating counterclockwise. The rotor is in edgewise flight, with the rotor's axis of rotation perpendicular to the freestream velocity. Figure 3a shows that in hover, where the advance ratio is near zero, all rotor blades experience advancing flow. Figures 3b and 3c show a region of reverse flow, as denoted by the region within the circle defined by the dashed line. The reduced velocity perpendicular to the leading edge of the retreating blade results in lower dynamic pressure, and a corresponding loss of thrust on the blade. In small amounts, the loss of thrust on the retreating blade can be compensated for by increasing the retreating blade's pitch via cyclic control. When the advance ratio becomes too great, typically around $\mu = 0.7$, compensating for the lack of dy-

[4] Advanced ratio is defined differently for propellers, the definition for propellers is $J = V_\infty/nD$, where n is the rotational speed in revolutions per second and D is the propeller diameter. The advance ratios are related, with $J = \pi\mu$.

[5] The leading edge is defined in the traditional sense. Thus, even if the flow is reversed and the trailing edge is facing the incoming velocity, it is still the trailing edge.

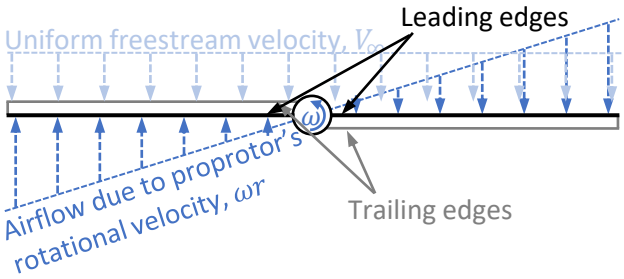

(a) Individual velocity components

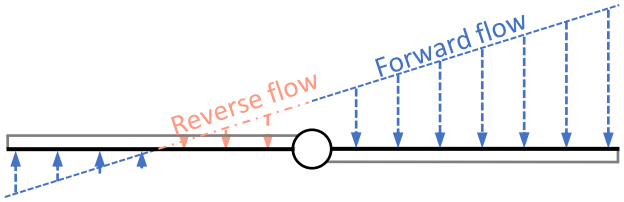

(b) Summed velocity components

Figure 2: The velocity vectors acting on the leading edge of a spinning proprotor blade during a moderate advance ratio. Note the reverse flow near the hub.

namic pressure on the retreating blade will drive the cyclic pitch to increase the section's angle of attack until it reaches its stall limit. At the stall limit, the retreating blade can no longer generate the same thrust as the advancing blade. This thrust differential results in a rolling moment for the vehicle that must be balanced through another means should the vehicle wish to travel faster. (For this reason, side-by-side rotor concepts [13] can achieve higher flight speeds due to the reduced need for the retreating blade to produce sufficient lift to counter the vehicle's rolling moment.)

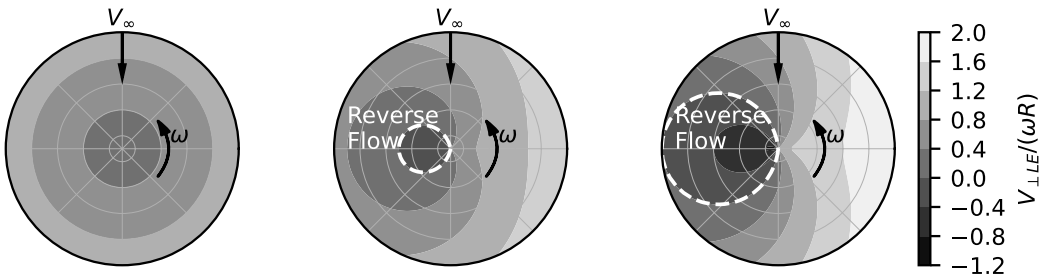

(a) $\mu \approx 0$ (b) $\mu = 0.5$ (c) $\mu = 1.0$

Figure 3: The velocity normal to the rotor's leading edge, normalized by tip velocity. Note that the region of reversed flow grows as advance ratio increases.

D. Inflow Angle with Variations in Advance Ratios

When the proprotor's axis of rotation lines up with the freestream velocity, such as during vertical climb, descent, or after conversion to forward flight (when acting like a propeller), there is no forward or retreating blade. (This memorandum always uses the rotor definition for advance ratio, defined by Eq. (7), rather than switching to the propeller definition of advance ratio to avoid confusion within the nomenclature.) The lack of a retreating blade removes the asymmetry shown

in Fig. 3, but proprotors are still limited in the maximum practical advance ratio when in axial flight. Consider the extremes of axial flow conditions, when the advance ratio is zero or infinite. At an advance ratio of zero, there is no velocity moving into the disk—except induced flow, which we neglect in this example—therefore, the blade will generate its maximum thrust when the chord line lies on the face of the disk, similar to a helicopter blade, albeit without any twist. When the advance ratio is very high, assume infinite, there would be little rotational velocity and predominantly forward axial velocity. This scenario essentially describes a fixed-wing aircraft's wing, and on these aircraft the airfoil chord points directly into the freestream, again neglecting any twist. Unfortunately, a wing in forward flight cannot generate thrust as the lift vector is perpendicular to the freestream.

An infinite advance ratio is infeasible, but the preceding discussion raises the question of what is the maximum practical advance ratio for axial flight. The upper limit on advance ratio is dictated by the need for the proprotor to perform across the operating range of advance ratios, and the greater this range, the more compromises must be made within the blade design. To understand the details, we must discuss the geometry of a proprotor's blade element and its inflow conditions.

Ignoring induced velocity—which may be a poor assumption—Eq. (8) relates the inflow angle across a blade, ϕ, to the advance ratio, μ. Within Eq. (8), r is the radial station and R is the blade radius. Figure 4 depicts the airfoil undergoing both forward and rotational velocity along with the associated blade element's angle of attack, α, and the blade pitch angle, θ. Equation (9) defines the blade pitch angle, which varies across the blade as it is the sum of the blade's geometric twist, which depends on radial station, and collective setting, which is constant across the blade.

$$\phi(r) = \arctan\left(\frac{\mu R}{r}\right) \tag{8}$$

$$\theta(r) = \beta(r) + \theta_c \tag{9}$$

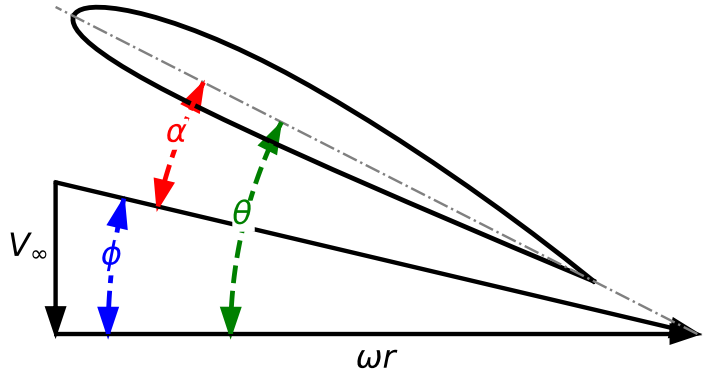

Figure 4: A proprotor blade section with both freestream velocity, V_∞, and rotational velocity, ωr, and related angles.

As noted earlier, proprotors in axial flight struggle to produce thrust at high advance ratios due to the rotation of the thrust vector with collective. The blade element generates a force normal to its chord, which has a coefficient C_{F_N}, in proportion to the product of its angle of attack and lift curve slope, C_{L_α}, i.e., $C_{F_N} \propto C_{L_\alpha}\alpha$. There is a corresponding tangential force generated by the blade element, with a coefficient C_{F_T}, defined by the blade element's drag. To produce thrust and torque, the normal and tangential vectors must be rotated by the collective to apply the forces in the appropriate directions. The rotations are effectively the same as for standard two-dimensional airfoils. Equations (10) and (11) highlight how the element's thrust, $\mathcal{T}$, and torque, Q, depend on

the blade pitch angle. During flight, the blade pitch angle is controlled through the collective as seen in Eq. (9). At high collectives, which are required for high advance ratio regardless of the blade twist, the proprotor's ability to produce thrust is diminished.

$$d\mathcal{T} \propto C_{L_\alpha}(\theta - \phi)\cos\theta - C_{F_T}\sin\theta \tag{10}$$

$$dQ \propto C_{L_\alpha}(\theta - \phi)\sin\theta + C_{F_T}\cos\theta \tag{11}$$

Figure 5a shows a plot of the inflow angle across the blade for various advance ratios, regardless of blade design and ignoring induced velocity. The upper and lower bounding advance ratios are shown in solid black lines with representative intermediate advance ratios shown in grey dashed lines. The limits do not represent the physical limits, a proprotor can have an advance ratio from zero to infinity. An advance ratio of zero implies hover or static operation whereas a practical upper bound for advance ratio is less than one due to the high blade pitch angle required. Thus, advance ratios from 0.1 to 0.9 represent a typical, or even expanded, range of advance ratios.

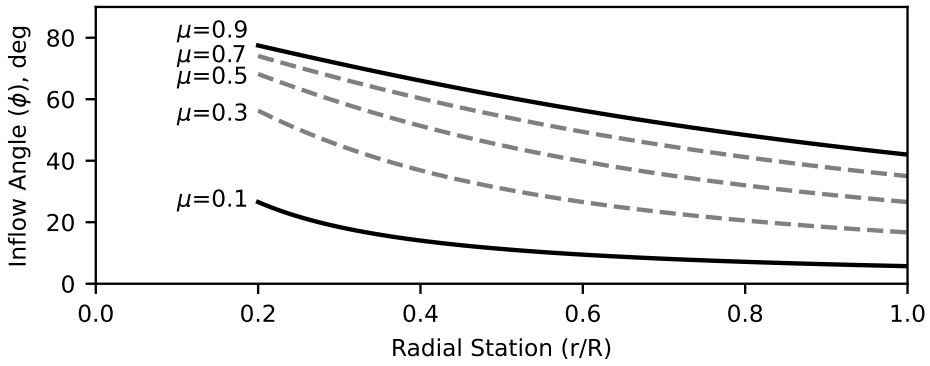

(a) The inflow angle coming into the proprotor blade as a function of advance ratio

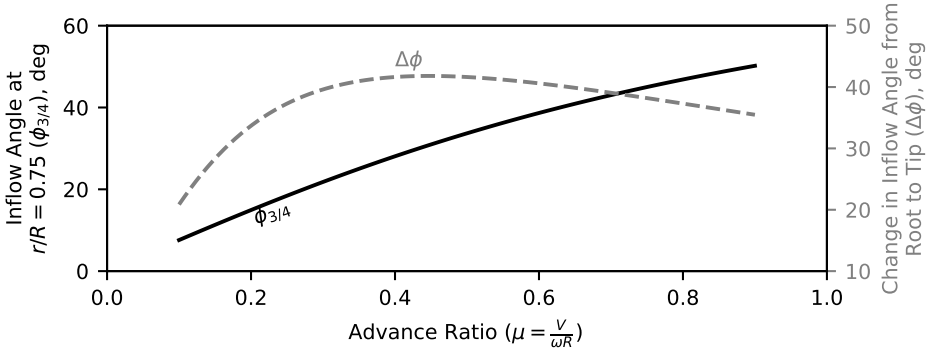

(b) Change in inflow angle at the 0.75 r/R station and the change in inflow angle from root to tip of a blade for different advance ratios

Figure 5: A proprotor must operate across a range of advance ratios, which impacts the inflow angle across the blade.

Ideally, the blade pitch angle would match the inflow angle such that the blade's angle of attack enables the section's L/D_{max}, which typically occurs at low, positive angles of attack. Of course, that is not possible due to the changing conditions across the blade for a range of advance ratios. A second design goal would be to avoid negative angles of attack such that the blade section always

generates positive thrust. (Cambered airfoils generate positive lift at negative angles of attack, provided the angles of attack are still close to zero.) Lastly, when possible, the airfoils should not operate at angles of attack that lead to stalled flow, as this increases the drag (or torque) on the proprotor, lowering the proprotor's efficiency. In effect, blades with significant stalled regions have low proprotor efficiencies and/or figures of merit.

There are two primary observations from Fig. 5a that are highlighted in Fig. 5b. Figure 5b shows the inflow angle at $r/R = 0.75$, or $\phi_{3/4}$, as a function of advance ratio.[6] The $\phi_{3/4}$ is a function of advance ratio, but the blade twist can easily accommodate changes in inflow angle at a single point via collective. The $\phi_{3/4}$ angle asymptotically approaches 90° as advance ratio approaches infinity,[7] and though the collective can help prevent blade stalling, high $\phi_{3/4}$ angles may still lead to low thrust production due to the observations from Eqs. (10) and (11).

The second observation is that the change in inflow angle from root to tip, $\Delta\phi$, varies in magnitude with advance ratio. Figure 6 shows the inflow angles for a "high" advance ratio of 0.7 and a "low" advance ratio of 0.1, at the root and tip stations. To emphasize the changes in blade twist required, the airfoils are superimposed atop the inflow angles such that the airfoils would be at an angle of attack of zero degrees. For the high advance ratio in Fig. 6a, the root of the blade is spinning slowly—ω is constant but r/R is small—whereas the tip is spinning rapidly. In this scenario, the inflow angle at the root—and thus the root airfoil's chord—would be more aligned with the axis of rotation and incoming velocity, while the tip's chord would be aligned with the proprotor disk. In this example, $\Delta\phi$ is high. Conversely, when the advance ratio is low, as shown in Fig. 6b, both the root and tip inflow angles are more aligned with the disk's plane and $\Delta\phi$ is low.

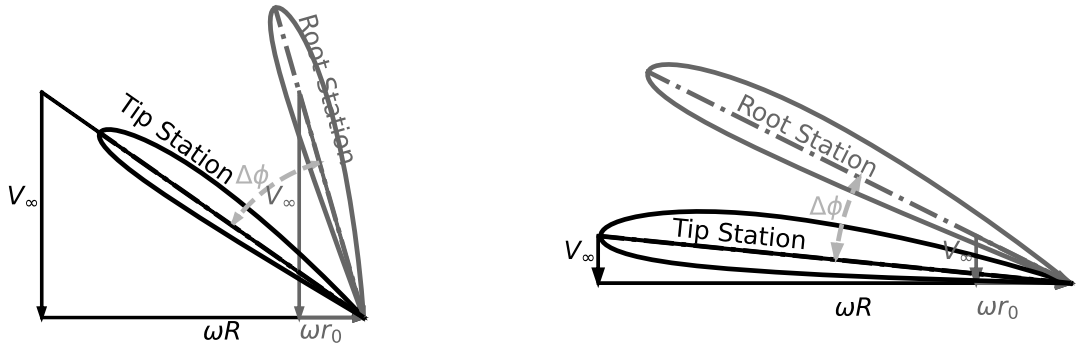

(a) Advance ratio of 0.7, $\Delta\phi = 39°$

(b) Advance ratio of 0.1, $\Delta\phi = 21°$

Figure 6: The change in ϕ from the root to the tip for two different advance ratios.

The change in inflow angle from root to tip reaches a maximum when $\mu = \sqrt{r_0/R}$, which is approximately 0.45 for a blade with $r_0/R = 0.2$. This is explained via the assumption that the inflow angle is an arctangent function.[8] Though a proprotor can match the inflow angle at one point on the blade via collective, there is no means to change the twist distribution in flight to match the inflow angle across the blade.[9] Thus, operating at any off-design condition will lead

[6] A proprotor generates most of its thrust near the tip, so the 3/4 position is commonly used as a reference point.

[7] The inflow angle, $\phi_{3/4}$ is described by the arctangent of advance ratio, $\phi_{3/4} \propto \arctan \mu$. Arctangent functions exhibit this behavior.

[8] Appendix A describes the math behind the relationship between the root chord station, advance ratio, and maximum change in inflow angle in more detail.

[9] Similar to variable camber wings in fixed-wing aircraft, adjustable twist rotors/propellers/proprotors are an active area of research to solve this problem.

to the blade sections operating at a relative angle of attack different than that of the maximum sectional lift-to-drag ratio. If the $\Delta\phi$ across the operating range of advance ratios is small, then the blade should perform well across its operating range; however, the difference in advance ratio from hover to forward flight is usually large and precludes good performance in both phases of flight. The topic of designing for hover and forward flight is addressed in the next section. Additionally, $\Delta\phi$ goes to zero as advance ratio goes to infinity, implying that under certain conditions, the hover and forward flight design points could have similar twist distributions because $\Delta\phi$ also goes to zero at hover (where the advance ratio is zero).

With a basic understanding of the incoming flow angle, ϕ, toward a proprotor blade, we can discuss how to adjust the geometric blade twist, β, to control the angle of attack, α, and obtain the desired proprotor performance. The ultimate goal is to balance the performance of the proprotor between its low and high advance ratio needs.

E. Design Example

To highlight some of the challenges in blade design, consider a proprotor blade expected to operate at hover and forward flight. Stoll provided early design details on the Joby S4 vehicle [14], with the salient parameters repeated in Table 1. The exact values for the parameters are not critical, and we assume that the rotor speed in cruise is half of that in hover based on past examples [2, 15].

Table 1: Example proprotor design specifications.

Parameter	Hover	Cruise
Rotor radius, ft	4.75	4.75
Rotor speed, rad/s	77.9	38.9
Flight speed, mph	0	200
Advance ratio (μ)	0	0.483

For this example, it is easier to specify a twist distribution that aligns with a certain advance ratio rather than a linear or piecewise-linear twist distribution. Effectively, this allows the angle of attack across the blade be zero[10] for a single advance ratio without having to specify the twist at the root and tip of the blade. Figure 7 shows the inflow angle across the proprotor blade at hover and cruise, with two notional blade designs, one closer to the forward flight (cruise) condition and the other closer to the hover condition. The blade twist distribution at the design advance ratio implies that the flow is aligned with the chord across the blade for this one condition.

To understand the aerodynamic behavior of the blade, let us allow the blade collective, θ_C, to vary as needed, with a θ_C = 0 when the blade is at its design point. When compared to its initial collective, negative collective decreases the angle of attack across the blade and a positive collective increases the angle of attack. As depicted in Fig. 4, the angle of attack that each blade section, r/R, sees is defined according to Eq. (12), where $\phi(r/R)$ is the inflow angle from Eq. (8), $\beta(r/R)$ is the geometric twist distribution, and θ_C is the collective input. Most airfoils will stall if the angle of attack is less than -15° or greater than 15°, and cambered airfoils will generate lift at angles of attack slightly below zero. We can use this knowledge to identify regions in which the proprotor will perform poorly.

[10] As previously stated, ideally the proprotor's blade would act at its maximum L/D angle of attack. For simplicity, the example assumes a zero degree angle of attack is sufficient.

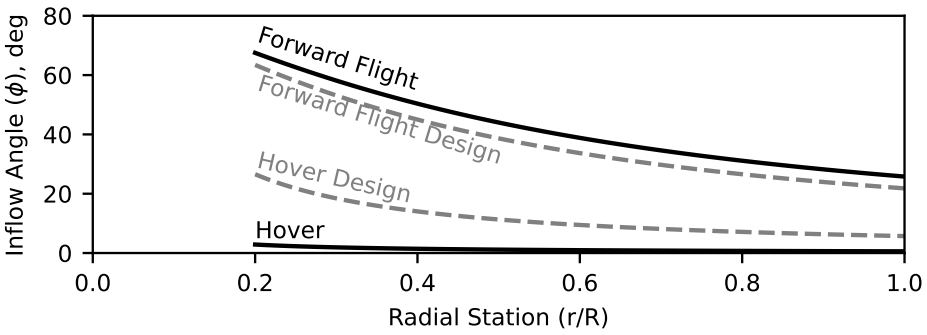

Figure 7: The example vehicle's inflow angles for its hover and cruise conditions, along with two potential design advance ratios.

$$\alpha(r/R) = \beta(r/R) - \phi(r/R) + \theta_C \tag{12}$$

Figure 8 shows a two-by-two matrix of proprotors designed for either hover or cruise, then operated at hover or cruise. The stalling and negative thrust angles of attack are identified with hash marks at the upper and lower portion of each graph, respectively. The collective settings were chosen such that the angle of attack in the outer portion of the blade would be (generally) in a region to produce thrust efficiently. Because this was an example to illustrate a challenge, no effort was made to optimize the thrust produced or find "ideal" collective settings. The use of two collective settings highlights the impact of raising or lowering the collective on the angle of attack.

Figure 8a shows a proprotor—designed for cruise and operating in hover—that has most of the blade operating in undesirable regions. With θ_C set to $-20°$, the tip is producing positive lift, but the blade becomes stalled inboard of $r/R = 0.55$. Setting the collective to $-30°$ allows for less of the inboard blade to be stalled, but the tip produces negative thrust. Having a stalled inboard portion may not be as deleterious to performance as a stalled outboard portion because the inboard portion of the blade produces less thrust due to the lower dynamic pressure than the outboard portion. Figure 8 shows the inboard station starting at $r/R = 0.2$, which implies that is the start of the airfoil shape. Inboard of this station, the proprotor's blade is transitioning from the hub attachment into the airfoil. A combination of low dynamic pressure and poor aerodynamic performance of the stations' cross sections leads to the inboard region contributing little to the blades' useful power. For helicopter rotors, whose blades are substantially longer than on propellers or proprotors, the innermost productive station will occur much lower than at $r/R = 0.2$.

Conversely, and as expected, when designed for, and operated in, the cruise condition, the blade is operating in an acceptable range of angles of attack across the blade. Figure 8b shows that the collective can operate over a range of angles without stalling any of the blade, and the required thrust can be adjusted based on collective and power. The designed blade would likely exhibit a high proprotor efficiency, η_p, in cruise but a low figure of merit in hover.

Figures 8c and 8d show the same information as Figs. 8a and 8b, except that in this scenario, the blades are designed for hover performance. As expected, the blades are within the acceptable range of angles of attack across the blade in hover, enabling the proprotor to generate the higher thrusts required in this phase. At cruise, the hover-designed blade shows an inboard region of negative thrust at the selected collectives, though these sections have a lower dynamic pressure and therefore a lower contribution to the total thrust than the outboard sections. Additionally, forward flight has a lower thrust requirement than hover, potentially permitting some regions of

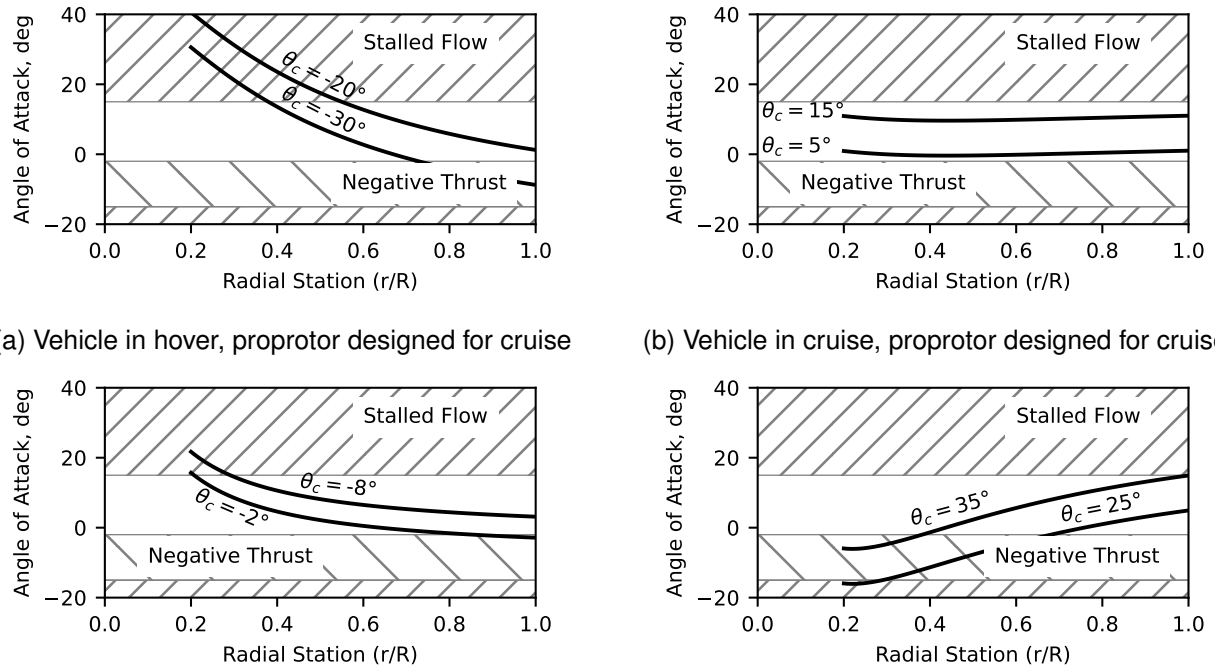

(a) Vehicle in hover, proprotor designed for cruise

(b) Vehicle in cruise, proprotor designed for cruise

(c) Vehicle in hover, proprotor designed for hover

(d) Vehicle in cruise, proprotor designed for hover

Figure 8: An example of the challenge designing a proprotor blade for hover and forward flight. Depending on the proprotor design, finding an operable range that balances the two extremes can be difficult.

negative thrust without sacrificing overall performance.

If the range of advance ratios could be narrowed, designing the blade for efficient operation would also be easier. However, the disparity in mission advance ratios is compounded by the fact that forward flight requires lower power, which is typically achieved through reducing the RPM, further increasing advance ratio. The mission profile and the split between hover time and cruise time will dictate which phase takes priority in the design. Hover-dominant vehicles, where most of the energy is consumed in hover, will benefit from skewing the design toward greater efficiency in that phase. Conversely, vehicles that travel longer distances in cruise will consume more energy at higher advance ratios and would benefit from skewing the design toward a cruise configuration.

F. Caveats

The preceding section described performance as if the operator has the ability to independently control velocity and rotor speed, which is not true. Forward velocity and rotor velocity are linked through the propulsor and proprotor model. In reality, the pilot (or control system, if unpiloted) directly controls the propulsor power and collective, not the rotor speed or torque. The proprotor's rotational speed is set when the torque required by the proprotor is equal to the torque output by the propulsor. It is possible that increasing the collective in an attempt to fly faster actually requires more torque and slows the proprotor's rotational speed, which decreases the vehicle's flight speed. As an example, setting the collective to 15° in Fig. 8b may actually lower thrust more than when the collective is set to five degrees because the increase in proprotor torque lowers the proprotor speed enough to offset the increase in angle of attack.

3. Chord and Thickness Distributions

The angle of attack of the proprotor blade is one piece of how the proprotor generates thrust. Another aspect is the chord distribution across the blade. The following subsections describe a process for creating a blade whose chord distribution varies linearly or quadratically with radial station. The purpose of the discussion is to identify the design space with which a blade can be shaped, such that trades against other disciplines, such as structures or acoustics, can be measured.

When discussing chord distributions, we often talk about rotor solidity, σ, and blade solidity, σ/B, where B is the number of blades. Solidity is simply the ratio of blade area to disk area, per Eq. (4). Equation (5) is the formula for calculating the blade area, which consists of taking the integral of the chord distribution as a function of radial station, $c(r)$, from root, r_0, to tip, R. The form of $c(r)$, whether that be linear (first order) or quadratic (second order), is the subject of the following sections.

A. Linear Chord Distributions

If we want to design a blade with a linear chord distribution, Eq. (13) describes the chord as a function of r where $c(r)$ is the chord distribution and c_1 and c_0 are constants. Solving for the coefficients requires two known parameters, an initial set can be the blade solidity and a specified chord somewhere along the blade. Using solidity and a chord length are good choices because they are commonly available early in the design process. Typically the blade solidity is estimated during the vehicle's initial sizing based on historical values, before detailed blade shaping is considered. An example of a specified chord could be a minimum root or tip chord. If a specific chord value along the blade is not known, we can still determine a small acceptable range of coefficient terms for use in parametric studies.

$$c(r) = c_1 r + c_0 \tag{13}$$

Figure 9 shows two blades with the same solidity and different c_1 terms. Figure 9a shows the geometry when c_1 is positive, also known as an inverse taper ratio. Conversely, the blade geometry in Fig. 9b has a a negative c_1 value, which is a traditional tapered blade. The combination of solidity and minimum root and/or tip chords may require the blade to have either a positive or negative c_1. If an inversely tapered blade is unacceptable, the designer must reevaluate other parameters in the design space. The following paragraphs describe the math required to determine the design space for blades with linear or constant chords.

(a) Minimum root chord

(b) Minimum tip chord

Figure 9: Proprotors designed with a linear chord distribution with a constraint on the minimum root or tip chord.

When considering chord distributions, there may be constraints on the minimum chord at the root or the tip; call these c_{r0} and c_R, respectively. Physically, the blade cannot have a negative chord length at any point on the blade, which means each of these values has an absolute lower limits of zero. In terms of Eq. (13), we can express these constraints via Eqs. (14) and (15). The solidity of the blade comes from inserting the chord equation, Eq. (13), into Eq. (5) and integrating

from root to tip to yield the blade area. The blade area can be used in Eq. (4) to find the rotor solidity. When expressed as blade solidity, the result is Eq. (16).

$$c_{r0} \leq c_1 r_0 + c_0 \tag{14}$$

$$c_R \leq c_1 R + c_0 \tag{15}$$

$$\frac{\sigma}{B} = \frac{1}{\pi R^2}\left(\frac{1}{2}c_1(R^2 - r_0^2) + c_0(R - r_0)\right) \tag{16}$$

Equations (14) – (16) are linear with respect to the coefficients, enabling us to understand the solution space of acceptable chord distributions. Figure 10 shows the solutions to Eqs. (14) – (16) with the c_1 term on the abscissa and c_0 on the ordinate axis. For a given solidity, the only viable chord distributions lie on the solid black line defined by the blade solidity equation. The minimum chord at the root and tip create a closed design space where only a small set of coefficients are valid. Increasing either minimum chord raises the constraint lines vertically. Linear coefficients (c_1) to the left of the origin imply a tapered blade, c_1 coefficients to the right of the origin imply a blade with inverse taper, and a $c_1 = 0$ is a rectangular blade.

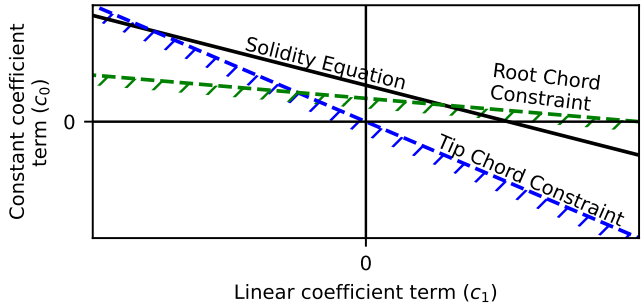

Figure 10: Solution space for linear coefficients defining the chord distribution. The constraint lines represent minimum chord at the root or tip. In this example, the tip chord minimum is zero, but the root chord minimum is a small, positive number.

Solving for the intersections of the solidity equation, Eq. (16), with either inequality, Eq. (14) or (15), yields Eqs. (17) and (18), which specify the slope of the chord distribution in terms of known blade parameters. These values for the linear term have corresponding values for the constant term, allowing us to define a range of blades with varying taper ratio that are guaranteed to meet the blade solidity requirement.

$$c_{1,min} = -\frac{2(\sigma - Bc_R(R - r_0))}{B(R - r_0)^2} \tag{17}$$

$$c_{1,max} = \frac{2(\sigma - Bc_{r0}(R - r_0))}{B(R - r_0)^2} \tag{18}$$

Rather than using linear equation coefficients, these relationships can be expressed in terms of the blade's taper ratio, λ_b, the tip chord, $c(R)$, and the root chord, $c(r_0)$. Equation (19) defines the taper ratio for a blade, and Eq. (20) specifies the solidity using the equation for the area of

a trapezoid. Using taper ratio is more intuitive for those familiar with wing design, though the preceding section provides a simpler example for when we consider quadratic chord distributions.

$$\lambda_b = \frac{c(R)}{c(r_0)} \tag{19}$$

$$\frac{\sigma}{B} = \frac{1}{2\pi R^2}(R - r_0)(c(R) + c(r_0)) \tag{20}$$

By rearranging the equations algebraically, we can compute the minimum and maximum taper ratio for a given solidity. Equations (21) and (22) express these relationships in terms of the minimum root or tip chord.

$$\lambda_{b,min} = \frac{c_R B(R - r_0)}{2\sigma - Bc_R(R - r_0)} \tag{21}$$

$$\lambda_{b,max} = \frac{2\sigma}{Bc_{r0}(R - r_0)} - 1 \tag{22}$$

B. Quadratic Chord Distribtions

We can extend the thought process for a linear chord distribution to quadratic chord distribution. Imagine we seek to design a rotor solidity per blade, σ/B, subject to minimum root and tip chords, c_{r0} and c_R. Physically, the root and tip chords must be greater than zero, though we can impose any minimum chord. Equation (23) defines the generic form of the chord distribution, $c(r)$, across the blade from root, $r = r_0$, to tip, $r = R$, where c_2, c_1, and c_0 are constants. Equations (24) and (25) show the first and second derivative of chord with respect to radial station, respectively.

$$c(r) = c_2 r^2 + c_1 r + c_0 \tag{23}$$

$$\frac{dc(r)}{dr} = 2c_2 r + c_1 \tag{24}$$

$$\frac{d^2c(r)}{dr^2} = 2c_2 \tag{25}$$

The value of c_2 controls the concavity of the blade, with Fig. 11 showing three blades with different c_2 values.[11] Figure 11a shows a blade with a negative c_2 value that results in a concave blade. Though it is physically possible to have a blade with a convex chord distribution, these are rarely used. Equation 24 controls the point of maximum chord, r_m, which mathematically could be anywhere if r in Eq. (23) can go to $\pm\infty$. Having a maximum chord outside of the blade, as Fig. 11b depicts, implies a more linear chord distribution for which the linear model is better suited. If a blade requires a quadratic chord distribution, it will superficially look like Fig. 11c, where the maximum chord occurs on the blade itself and the blade has a concave shape.

To make the problem tractable, let us assume that the chord distribution has concavity (a negative c_2 value), otherwise the blade would be thinner at the mid-span than the root or tip. Additionally, assume the maximum chord lies at or between the root and the tip at a position r_m.

[11] In this discussion, concave refers to a blade that has a maximum chord location somewhere along the blade. This definition coincides with the mathematical definition and implies that Eq. 23 is concave if the second derivative, i.e., c_2, is negative. Conversely, if the c_2 is positive, the blade has a convex chord distribution and the blade will have a minimum chord along its blade.

(a) Concave chord distribution (b) "Linear" chord distribution (c) Concave chord distribution

Figure 11: Changes in chord distribution depending on the c_2 value.

Using calculus again, we can set the left side of Eq. (24) to zero to yield the position of maximum chord. Equation (26) shows the result, in which c_2 and c_1 must be related.

$$c_1 = -2c_2 r_m \tag{26}$$

We can find the blade area by substituting Eq. (23) into Eq. (5) and integrating along the blade via the power rule, resulting in Eq. (27). To reduce the number of coefficients, we substitute Eq. (26) into Eq. (27). We can substitute this relation for A_b into the solidity equation, Eq. (4), combine terms, then reorganize the equation to solve for c_0, as shown in Eq. (28). Equation (28) relates the c_2 and c_0 terms such that choosing a value for either will define the chord distribution that satisfies the blade solidity requirement. Equation (28) does not ensure that the root or tip chord minimums are met; however, it allows us to visualize the design space for the chord distribution.

$$A_b = \frac{1}{3}c_2(R^3 - r_0^3) + \frac{1}{2}c_1(R^2 - r_0^2) + c_0(R - r_0) \tag{27}$$

$$c_0 = \frac{\sigma\pi R^2}{B(R - r_0)} - \frac{1}{3}c_2(R^2 + Rr_0 + r_0^2) + c_2 r_m(R + r_0) \tag{28}$$

Figure 12 shows the solution space for c_2 (the non-linear coefficient) and the radial station of the maximum chord. The value in having this visual is that one could run a set of proprotor performance measurements and understand how changes in chord distribution impact the final metric. The design conditions in Fig. 12 are for a proprotor with four blades and a solidity of 0.2. The constraints on the root and tip chord, as a fraction of blade radius, c/R, are 5% for the root and 0% for the tip, i.e., the tip can come to a point. Depending on the specifics of the geometry, Fig. 12 will shift, but the trends remain. The upper bound on the plot is where the blade has no concavity and is effectively a linear blade. The figure helps identify if there are no feasible blade solutions, or what the impact of relaxing a chord length requirement would be on the design space.

C. Thickness Distribution

Aerodynamically, the thickness distribution is of less consequence than the chord or twist distribution. Rather, it is structural or acoustical considerations that drive the thickness distribution. Inboard, where the stresses are highest, the blade will be thickest. Where the blade attaches to the hub, the blade is typically round, and it transitions into an airfoil around the $r/R = 0.2$ radial section. The result is that the inboard section maintains a higher thickness-to-chord than the outer sections. The blade thickness-to-chord ratio does impact the Mach drag divergence, with lower thickness-to-chord ratios having higher Mach numbers before drag rise begins [16]. Between the structural concerns near the root and high speed flow near the tip, proprotors will have monotonically decreasing thickness-to-chord ratios from root to tip.

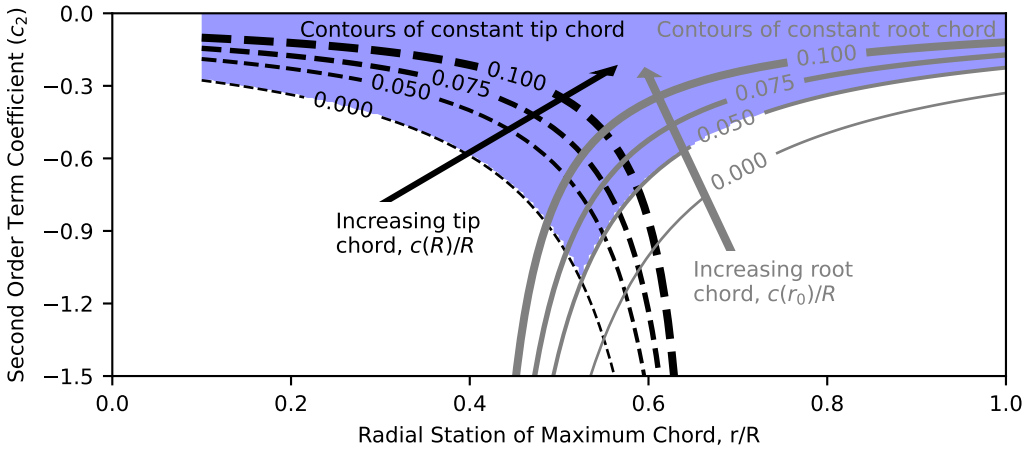

Figure 12: Solution space for quadratic coefficients defining the chord distribution. The solid lines are constant root chord lengths normalized by proprotor radius, and the dashed lines are constant tip chord lengths normalized by the proprotor radius. The filled region above the lines is a viable solution space meeting an arbitrary minimum root and tip chord length.

4. Concluding Remarks

This technical memorandum summarizes some of the basic aerodynamic considerations that drive the design of a proprotor. Aerodynamics is one facet of a complete design and must be considered in parallel with other disciplines such as structures and acoustics. The work within this technical memorandum assumes rigid blades and does not account for the lack of structural integrity that may result from overly thin blades. Similarly, a pure aerodynamic design may yield an acoustically unacceptable design. The result is that this memorandum should be considered for education and general design principles. Adhering strictly to the equations listed herein will result in unrealistic blades that are ill suited for actual proprotors.

This memorandum does not address induced losses that come from the thrust distribution across the blade. The goal of most proprotor designs is to minimize the induced losses on each blade. Induced losses are analogous to induced drag on a fixed-wing aircraft and result from the same physics. In the same way that careful design of the lift distribution on a wing can reduce induced drag, the design of the thrust distribution on a proprotor can reduce a proprotor's induced losses. Proprotors employing this thrust distribution are called minimum induced loss (MIL) proprotors, and there are existing codes to design proprotors for this condition using blade element momentum theory (BEMT) approaches. An MIL state can only be achieved at a single operating point, implying that a robust design would be more appropriate for a proprotor that must operate over a range of conditions.

5. Future Work

The final step is to put the design approaches for twist and chord distribution into practice and design a proprotor that has "sufficient" performance across its flight envelope, weighted to reduce energy consumption. This design will yield an aerodynamic-centric result, with little regard for what may be an acoustically or structurally acceptable proprotor. The goal is that this process could be incorporated into a broader toolchain to trade aerodynamic performance with acoustic and structural performance.

Appendices

A. Inflow Angles

The inflow angle of a proprotor in axial flight with no slip or induced velocity is an arctangent function based on the two velocity vectors. For simplicity, assume that the blade radius is one, thus $r = r/R$. Equation (29) repeats Eq. (8) from the main text with $R = 1$, Eq. (30) shows its partial derivative with respect to radial station, r, and Eq. (31) shows its partial derivative with respect to advance ratio, μ.

$$\phi(r, \mu) = \arctan\left(\frac{\mu}{r}\right) \tag{29}$$

$$\frac{\partial \phi(r, \mu)}{\partial r} = \frac{-\mu}{\mu^2 + r^2} \tag{30}$$

$$\frac{\partial \phi(r, \mu)}{\partial \mu} = \frac{r}{r^2 + \mu^2} \tag{31}$$

Equation (32) shows the equation for the change in inflow angle from root to tip, where r_0 is the root radial station. Proprotor blades cannot maintain an airfoil section all the way to the hub. A typical r_0 value is 0.2. Differentiating Eq. (32) with respect to μ, yields Eq. (33).[12] To find the advance ratio that leads to the largest change in inflow angle from root to tip, set the left side of Eq. (33) equal to zero and solve for the advance ratio. The result is that when the advance ratio reaches the square root of the root radial section, i.e. $\mu = \sqrt{r_0}$, the change in inflow angle will be at a maximum.

$$\Delta\phi = \arctan\left(\frac{\mu}{r_0}\right) - \arctan(\mu) \tag{32}$$

$$\frac{\partial \Delta\phi}{\partial \mu} = \frac{r_0}{r_0^2 + \mu^2} - \frac{1}{1 + \mu^2} \tag{33}$$

B. Ideal Proprotor Loading

Fundamental momentum theory describes the proprotor as an actuator disk with a static pressure jump. Using this approximation, the thrust generated by a proprotor, $\mathcal{T}$, is the product of the change in static pressure across the proprotor, Δp, and the proprotor's area, A, as shown in Eq. (34).

$$\mathcal{T} = A\Delta p \tag{34}$$

Within the flow, the stagnation pressure is constant upstream and downstream of the actuator disk but not across it because the actuator disk acts as a source term in the flow. Equation (35) shows the relationship upstream and downstream of the proprotor, which we can rearrange to Eq. (36) to determine the induced velocity, V_2.

$$p_\infty + \frac{1}{2}\rho V_\infty^2 + \Delta p = p_\infty + \frac{1}{2}\rho V_2^2 \tag{35}$$

$$V_2 = \sqrt{\frac{2\Delta p}{\rho} + V_\infty^2} \tag{36}$$

[12] Using the derivative of Eq. (31) as an example.

Equation (37) shows the Froude efficiency, η_p, of an ideal proprotor in its canonical form, though we can replace V_2 with the relation obtained in Eq. (36) to yield the efficiency in terms of Δp as Eq. (38) shows. As we would expect, if Δp goes to zero, the efficiency goes to one.

$$\eta_p = \frac{2}{1 + \frac{V_2}{V_\infty}} \tag{37}$$

$$\eta_p = \frac{2}{1 + \frac{\sqrt{\frac{2\Delta p}{\rho} + V_\infty^2}}{V_\infty}} \tag{38}$$

Let us assume we have N proprotors, each with area A_i. The target thrust for the entire system is $\mathcal{T}$, which we can distribute across the proprotors in any fashion. The fraction of the total thrust put on an individual proprotor is κ_i, as shown in Eq. (39). Thus, the sum of κ_i from $i = 1$ to $i = N$ is one. Similarly, Eq. (40) describes the shaft power consumed by each proprotor, $P_{s,i}$.

$$\mathcal{T}_i = \kappa_i \mathcal{T} \tag{39}$$

$$P_{s,i} = \frac{\kappa_i \mathcal{T} V_\infty}{\eta_{p,i}} \tag{40}$$

The goal is to minimize the total shaft power, which Eq. (41) describes mathematically.

$$\begin{aligned} \underset{\kappa_i}{\text{minimize}} \quad & \sum_{i=1}^{N} P_{s,i} \\ \text{subject to} \quad & \sum_{i=1}^{N} \kappa_i = 1 \end{aligned} \tag{41}$$

We can solve for the thrust scaling factor via Lagrangian multipliers. Equation (42) shows the Lagranian, which is only a function of κ_i.

$$\mathcal{L} = \frac{\kappa_i \mathcal{T} V_\infty}{\eta_{p,i}} + \lambda \left(\sum_{i=1}^{N} 1 - \kappa_i \right) \tag{42}$$

The gradient is simply the partial derivative with respect to κ_i, which simplifies to the expression in Eq. (43).

$$\frac{\partial \mathcal{L}}{\partial \kappa_i} = \frac{\mathcal{T} V_\infty}{\eta_{p,i}} - \lambda \tag{43}$$

The solution occurs when the left hand side of Eq. (43) is zero. Because λ is a constant, Eq. (43) is only zero when $\eta_{p,i}$ is constant. In order for each proprotor efficiency to be equal, Eq. (38) says each proprotor must have the same Δp across its actuator disk. Via Eq. (34), the thrust carried on each proprotor is $A_i \Delta p$, which leads us to the relationship for κ_i in Eq. (44), where A_t is the total propulsor area.

$$\kappa_i = \frac{A_i}{A_t} \tag{44}$$

The derived relationship for thrust distribution across a set of proprotors is important for two reasons. The first is that it easily relates the optimal thrust to the area of the proprotor. The second is that it states each proprotor should have the same pressure jump and proprotor efficiency, which implies that we can combine all the proprotors into one equivalent proprotor with the equivalent

total area. By combining the system of proprotors into one equivalent proprotor, we can determine the effect on η_p from increasing the proprotor area. We do this by rearranging Eq. (37) in terms of thrust per area to yield Eq. (45). Because the area terms are in the denominator of the fraction, we can see that adding area brings diminishing returns to proprotor efficiency.

$$\frac{\partial \eta_p}{\partial A} = \frac{2\mathcal{T} V_\infty}{\rho \sqrt{\frac{2\mathcal{T}}{\rho A} + V_\infty^2} \left(\sqrt{A \left(\frac{2\mathcal{T}}{\rho} + V_\infty^2 A \right)} + V_\infty A \right)} \tag{45}$$

References

[1] Whiteside, S. K. S., Pollard, B. P., Antcliff, K. R., Zawodny, N. S., and Fei, X., "Design of a Tiltwing Concept Vehicle for Urban Air Mobility," Technical Memorandum NASA/TM-20210017971, NASA, Jun. 2021. doi: https://ntrs.nasa.gov/citations/20210017971.

[2] Radotich, M., "Conceptual Design of Tiltrotor Aircraft for Urban Air Mobility," *Aeromechanics for Advanced Vertical Flight Technical Meeting, Transformative Vertical Flight*, Vertical Flight Society, San Jose, CA, 2022.

[3] Gessow, A., "Effect of Rotor-Blade Twist and Plan-Form Taper on Helicopter Hovering Performance," Technical Note 1542, National Advisory Committee for Aeronautics, Feb. 1948.

[4] Fitzgibbon, T., Woodgate, M., and Barakos, G., "Assessment of Current Rotor Design Comparison Practices Based on High-Fidelity CFD Methods," *The Aeronautical Journal*, Vol. 124, No. 1275, 2020, pp. 731–766. doi: https://doi.org/10.1017/aer.2019.162.

[5] Litherland, B. L., Borer, N. K., and Zawodny, N. S., "X-57 "Maxwell" High-Lift Propeller Testing and Model Development," No. 2021-3193 in AIAA AVIATION Forum, American Institute of Aeronautics and Astronautics, 2021. doi: https://doi.org/10.2514/6.2021-3193.

[6] Critchfield, T., and Ning, A., "Low-Fidelity Design Optimization and Parameter Sensitivity Analysis of Tilt-Rotor eVTOL Electric Propulsion Systems," No. 2023-0325 in AIAA SciTech, American Institute of Aeronautics and Astronautics, 2023. doi: https://doi.org/10.2514/6.2023-0325.

[7] Clarke, M. A., and Botero, E., "Aeroacoustic Optimization of VTOL Rotor Blades," No. 2023-0209 in AIAA SciTech, American Institute of Aeronautics and Astronautics, 2023. doi: https://doi.org/10.2514/6.2023-0209.

[8] Gur, O., *Propeller Design*, American Institute of Aeronautics and Astronautics, Reston, VA, 2024.

[9] McVeigh, M. A., Rosenstein, H. J., and McHugh, F. J., "Aerodynamic Design of the XV-15 Advanced Composite Tilt Rotor Blade," Forum 39, Vertical Flight Society, 1983.

[10] Bain, J., Mikić, G. V., and Stoll, A., "Aerodynamic and Acoustic Design of the Joby Aviation eVTOL Propeller," No. 2021-16687 in Forum 77, Vertical Flight Society, 2021.

[11] Maisel, M. D., Giulianetti, D. J., and Dugan, D. C., "The History of the XV-15 Tilt Rotor Research Aircraft: From Concept to Flight," *Monographs in Aerospace History #17*, NASA SP-2000-4517, NASA, 2000.

[12] Leishman, J. G., *Principles of Helicopter Aerodynamics*, Cambridge Aerospace Series, The Pitt Building, Trumpington St, Cambridge, UK, 2000.

[13] Silva, C., Johnson, W. R., Patterson, M. D., and Antcliff, K. R., "VTOL Urban Air Mobility Concept Vehicles for Technology Development," No. 2018-3847 in AIAA AVIATION Forum, American Institute of Aeronautics and Astronautics, 2018. doi: https://doi.org/10.2514/6.2018-3847.

[14] Stoll, A., "Analysis and Full Scale Testing of the Joby S4 Propulsion System," *Second Annual Transformative Vertical Flight Concepts Workshop: Enabling New Flight Concepts Through Novel Propulsion and Energy Architectures*, NASA/CP-2016-219141, NASA, 2015. URL https://nari.arc.nasa.gov/sites/default/files/attachments/Stoll-TVFW-Aug2015.pdf.

[15] Schleicher, D. R., Phillips, J. D., and Carbajal, K. B., "Design Optimization of High-Speed Proprotor Aircraft," NASA Technical Memorandum NASA-TM-103988, NASA, Apr. 1993.

[16] Mason, W., "Analytic Models for Technology Integration in Aircraft Design," No. 1990-3262 in AIAA/AHS/ASEE Aircraft Design, Systems and Operations Conference, American Institute of Aeronautics and Astronautics, 1990. doi: https://doi.org/10.2514/6.1990-3262.